




Er-driven incommensurate to commensurate magnetic phase transition of Fe in the spin-chain compound BaErFeO₄

Andreas Dönni ¹, Vladimir Y. Pomjakushin ², and Alexei A. Belik ^{1,*}

¹Research Center for Materials Nanoarchitectonics (MANA), National Institute for Materials Science (NIMS), Namiki 1-1, Tsukuba, Ibaraki 305-0044, Japan

²Laboratory for Neutron Scattering and Imaging, Paul Scherrer Institute, 5232 Villigen PSI, Switzerland



(Received 18 September 2023; revised 30 November 2023; accepted 8 January 2024; published 2 February 2024)

Magnetic phase transitions and structures of the spin-chain compound BaErFeO₄ were investigated by measurements of magnetic properties (specific heat, magnetic susceptibility) and neutron diffraction. The lattice geometry of the orthorhombic crystal structure (space group *Pnma*) of the BaRFeO₄ compounds ($R = \text{Dy–Yb, Y}$) supports frustrations which lead to multiple magnetic phase transitions with complex magnetic structures. BaErFeO₄ undergoes three successive magnetic phase transitions at $T_{N1} = 49$ K, $T_{N2} = 33.4$ K, and $T_{N3} = 3.4$ K. In contrast with the previously investigated BaRFeO₄ ($R = \text{Y, Tm, Yb}$) compounds, all with incommensurate magnetic propagation vectors $\mathbf{k}_1 = (0, 0, k_z)$, BaErFeO₄ is the first member in this series that shows a phase transition from an incommensurate (\mathbf{k}_1 below T_{N1}) to a commensurate magnetic structure with $\mathbf{k}_2 = (\frac{1}{2}, 0, \frac{1}{2})$ below T_{N2} . In the crystal structure, all magnetic ions (Fe1, Fe2, Er1, and Er2) are part of chains propagating along the *b* axis. Below T_{N1} , strong antiferromagnetic (AFM) Fe-Fe spin-exchange coupling between square pyramidal (Fe1) and octahedral (Fe2) centers generates a collinear AFM structure with a constant size of the ordered Fe moments and a constant magnetic phase inside each chain of Fe³⁺ cations. Exchange coupling between the Fe chains is much weaker. At T_{N2} , *3d-4f* exchange interactions induce an ordered moment at the Er³⁺ ions, which results in a change of the direction of the ordered Fe moments from the *b* direction (above T_{N2}) to inside the *ac* plane (below T_{N2}) and a change from an incommensurate (\mathbf{k}_1 above T_{N2}) to a commensurate (\mathbf{k}_2 below T_{N2}) AFM structure. Toward lower temperature, *4f-4f* exchange interactions become stronger and create at T_{N3} a constant magnetic phase inside each chain of Er³⁺ cations. At T_{N2} and T_{N3} , the magnetic susceptibility shows sharp decreases that coincide with large increases of the correlation length of the magnetic structure. The unique magnetic structures of BaErFeO₄ are compared with those of other BaRFeO₄ compounds by considering experimental and theoretical aspects.

DOI: [10.1103/PhysRevB.109.064403](https://doi.org/10.1103/PhysRevB.109.064403)

I. INTRODUCTION

First-principles calculations are powerful enough to predict correct crystal ground-state structures of many materials [1], but they are not yet capable of predicting real magnetic ground states; they can only give the lowest-energy structure among different calculated models. Neutron diffraction is a unique direct method to determine the magnetic structure of a crystal. Magnetic structure solutions from neutron diffraction are still mainly a trial-and-error approach to fit the experimental data to all possible symmetry-adapted magnetic structures (representation analysis, calculated by a computer program) for a given crystal structure and a propagation vector (a point on the Brillouin zone) [2–4].

Magnetic exchange interactions between *3d* and *4f* electrons may account for complex magnetic properties of intermetallic compounds, as illustrated by recent examples based on neutron diffraction. In the centrosymmetric green phase compound Gd₂BaCuO₅ [5], the coupling of Cu²⁺ and Gd³⁺ spins is important in inducing ferroelectricity. The interplay of *3d-4f* interactions demonstrates an alternative

route to find magnetoelectric materials. In the Mn self-doped perovskite (Yb_{0.667}Mn_{0.333})MnO₃ [6], Yb–Yb interactions create an antiferromagnetic (AFM) structure at $T_N \approx 40$ K, whereas Mn–Yb interactions induce a small but nonzero ferromagnetic (FM) Yb³⁺ moment at much higher temperature ($T_c = 106$ K).

We have recently started to investigate the rare-earth series of isostructural quarternary ferrites, BaRFeO₄ with $R = \text{Dy to Yb}$ [7,8], and found that each compound shows unique magnetic and dielectric properties. Detailed magnetic, dielectric, and ferroelectric properties of BaHoFeO₄ were investigated by other authors [9,10], and the appearance of a hidden multiferroic state under a magnetic field has been discovered [9]. Members of the BaRFeO₄ series are isostructural with the parent compound BaYFeO₄ [11–16], which undergoes two successive magnetic phase transitions at $T_{N1} = 48$ K and $T_{N2} = 36$ K. Below T_{N2} , a cycloidal incommensurate magnetic structure and a spin-driven multiferroic state have been observed [12,13]. Due to the peculiar orthorhombic crystal structure, where magnetic ions form spin chains, BaRFeO₄ ferrite compounds exhibit multiple phase transitions and adopt complex magnetic structures. Recently, we have determined the magnetic structures of the compounds BaYbFeO₄ and BaTmFeO₄ [17] with three successive magnetic phase

* alexei.belik@nims.go.jp

transitions and found that $3d$ - $4f$ magnetic exchange interactions play an important role. Based on neutron diffraction experiments, all magnetic structures of the parent compound BaYFeO_4 [12] and BaRFeO_4 ($R = \text{Yb, Tm}$) [17] were found to be incommensurate with a magnetic propagation vector $\mathbf{k}_1 = (0, 0, k_z)$.

In this paper, we present measurements of specific heat, magnetic susceptibility, and neutron diffraction to extend the determination of the magnetic structures to BaErFeO_4 with three successive magnetic phase transitions at $T_{N1} = 49$ K, $T_{N2} = 33.4$ K, and $T_{N3} = 3.4$ K. BaErFeO_4 is found to be the first member in the series of BaRFeO_4 ferrites that shows a phase transition from an incommensurate magnetic structure with $\mathbf{k}_1 = (0, 0, k_z)$ below T_{N1} to a commensurate magnetic structure with $\mathbf{k}_2 = (\frac{1}{2}, 0, \frac{1}{2})$ below T_{N2} . Magnetic exchange interactions among and between $3d$ and $4f$ electron spins have different strengths and shape the magnetic structures at different temperatures. Here, $3d$ - $3d$ coupling at T_{N1} , T_{N2} , and T_{N3} , $3d$ - $4f$ interactions at T_{N2} , and $4f$ - $4f$ coupling at T_{N3} . Magnetic properties of BaErFeO_4 with sharp decreases of the magnetic susceptibility at T_{N2} and T_{N3} are unique in the series of BaRFeO_4 ferrites.

II. EXPERIMENTAL

A large amount (~ 11 g) of polycrystalline BaErFeO_4 ferrite sample was synthesized from stoichiometric mixtures of BaCO_3 (99.9%), Er_2O_3 (99.9%), and Fe_2O_3 (99.999%) using a conventional solid-state annealing method. The obtained mixture was pressed into pellets and annealed in air on Pt foil successively at (1) 1430 K for 40 h, (2) 1520 K for 30 h, (3) 1520 K for 36 h, and (4) 1520 K for 40 h, with grinding between each of the four steps. The resulting BaErFeO_4 sample contained no detectable impurity phase based on x-ray and neutron diffraction data. All measurements reported in this paper were performed on this BaErFeO_4 ferrite sample.

To investigate the magnetic phase transitions, the specific heat of BaErFeO_4 was measured in several magnetic fields from 0 to 90 kOe at temperatures between 2 K and room temperature using a commercial calorimeter (Quantum Design PPMS) by the pulse relaxation method. Magnetic susceptibility measurements were performed on a SQUID magnetometer (Quantum Design MPMS-XL-7 T) at temperatures between 2 and 400 K on cooling and warming in applied magnetic fields from 0.1 to 10 kOe.

To determine the magnetic structures of BaErFeO_4 , powder neutron diffraction experiments were performed at the Paul Scherrer Institute, Switzerland, on the high-resolution powder diffractometer for thermal neutrons (HRPT) [18] using an incident neutron wavelength of $\lambda = 1.886$ Å. Data were collected in the magnetically ordered and paramagnetic states at temperatures between 1.8 and 70 K for a 2θ range of 3.55° – 164.50° and a step width of 0.05° . We did not measure the experimental absorption correction coefficient μR of our BaErFeO_4 sample. Er has a moderate macroscopic absorption cross-section per unit volume Σ of 5.1861 cm^{-1} [19], relative to huge values of some other rare-earth elements, such as Dy (29.731 cm^{-1}), Sm (171.23 cm^{-1}), or Gd (1494.1 cm^{-1}). A rough estimation gives $\mu R \sim 0.8 (= 5.1861 \times 0.394 \times 0.4)$ based on an atomic mass ratio of 39.4% of Er in BaErFeO_4

and $R = 0.4$ cm of the cylindrical sample holder. The diffraction patterns were analyzed with $\mu R = 0.8$ by the Rietveld method using the FULLPROF suite [20]. The peak shape function used in the refinements was Thompson-Cox-Hastings pseudo-Voigt convoluted with axial divergence asymmetry function [21]. Possible models for the magnetic structures were deduced based on a group theory analysis using the programs ISODISTORT [22] and BASIREPS in the FULLPROF suite program package [20].

III. RESULTS AND DISCUSSION

A. Crystal structure of BaErFeO_4

The crystal structure of BaErFeO_4 at room temperature has been determined by synchrotron x-ray diffraction [8]. BaErFeO_4 crystallizes in the orthorhombic space group $Pnma$ (No. 62) and is isostructural with BaYFeO_4 [11]. The BaYFeO_4 structure type is formed for BaRFeO_4 compounds with $R = \text{Dy} - \text{Yb}$ [7,8]. The structure parameters of paramagnetic BaErFeO_4 at $T = 70$ K refined from powder neutron diffraction data are summarized in Table I. They are in good agreement with the reported room-temperature synchrotron x-ray results [8]. Refinements performed for different values of the absorption correction coefficient ($0.0 \leq \mu R \leq 2.0$) showed a strong correlation with the Debye Waller factors and no correlation for the other structural parameters (values within the errors given in Table I) and the agreement values of the fit. As a conclusion, except for the Debye-Waller factors, Er absorption can be neglected in the crystal structure refinement.

The arrangement of the magnetic ions (Fe1, Fe2, Er1, and Er2) in the crystal structure of BaErFeO_4 is shown in Fig. 1 as a projection onto the bc and ac planes. All magnetic ions are all located on $4c$ sites ($x, \frac{1}{4}, z$) with the structure parameters given in Table I. There are rings consisting of 4 magnetic ions [for example, Fe₂₁, Fe₁₂, Fe₂₃, and Fe₁₄, see Fig. 1(b)], and each ring forms a chain propagating along the b axis. All magnetic ions are part of rings and chains. The orthorhombic crystal structure of BaErFeO_4 is illustrated in Fig. 2. The chains of Fe^{3+} ions are built by alternate corner shared units of $[\text{FeO}_5]^{7-}$ square pyramids (Fe1, blue) and $[\text{FeO}_6]^{9-}$ octahedra (Fe2, red) [11].

Figure 3 shows the temperature dependence of the lattice constants a , b , and c and the volume V of BaErFeO_4 below $T = 70$ K based on our neutron diffraction data. For all parameters, a monotonic decrease is observed in the commensurate magnetic phase below T_{N2} . When decreasing the temperature from the paramagnetic state ($T = 70$ K) to the incommensurate magnetic phase (between T_{N1} and T_{N2}), spin-lattice coupling creates a small increase for the lattice constant b but not for a , c , and V .

B. Magnetic phase transitions of BaErFeO_4

Figures 4 and 5 show the temperature dependence of the specific heat C_p/T at different magnetic fields. No specific heat anomaly was observed at T_{N1} during the transition to the incommensurate magnetic phase in agreement with results for other members of the BaRFeO_4 family ($R = \text{Y}$ [7], Dy [7], and Ho [9]). A very weak specific heat anomaly was detected

TABLE I. Structure parameters of paramagnetic BaErFeO₄ at $T = 70$ K refined from powder neutron diffraction data (HRPT, $\lambda = 1.886$ Å, $\mu R = 0.8$). Space group $Pnma$ (No. 62); $Z = 8$. WP: Wyckoff position. The occupation factor $g = 1$ for all the sites.

BaErFeO₄, $T = 70$ K:

$a = 13.0844(1)$ Å; $b = 5.6736(1)$ Å; $c = 10.2055(1)$ Å; $V = 757.62(1)$ Å³.

$\chi^2 = 3.73$; $R_{wp} = 2.57\%$; $R_{exp} = 1.33\%$; $R_{Bragg} = 2.35\%$.

Site	WP	x	y	z	$B(\text{Å}^2)$
Ba1	4c	0.2110(2)	0.25	0.6738(3)	$=B(\text{Er}1)$
Ba2	4c	0.4146(3)	0.25	0.3956(3)	$=B(\text{Er}1)$
Er1	4c	0.4147(1)	0.25	0.0140(2)	0.26(2)
Er2	4c	0.1435(1)	0.25	0.3102(2)	$=B(\text{Er}1)$
Fe1	4c	0.4681(1)	0.25	0.7156(1)	0.24(2)
Fe2	4c	0.1902(1)	0.25	0.0227(1)	$=B(\text{Fe}1)$
O1	4c	0.5867(3)	0.25	0.6156(2)	0.49(2)
O2	4c	0.2907(2)	0.25	0.1820(3)	$=B(\text{O}1)$
O3	8d	0.0056(1)	0.5093(3)	0.3597(1)	$=B(\text{O}1)$
O4	8d	0.2175(1)	0.5086(3)	0.4408(1)	$=B(\text{O}1)$
O5	8d	0.1117(1)	0.0000(4)	0.1312(1)	$=B(\text{O}1)$

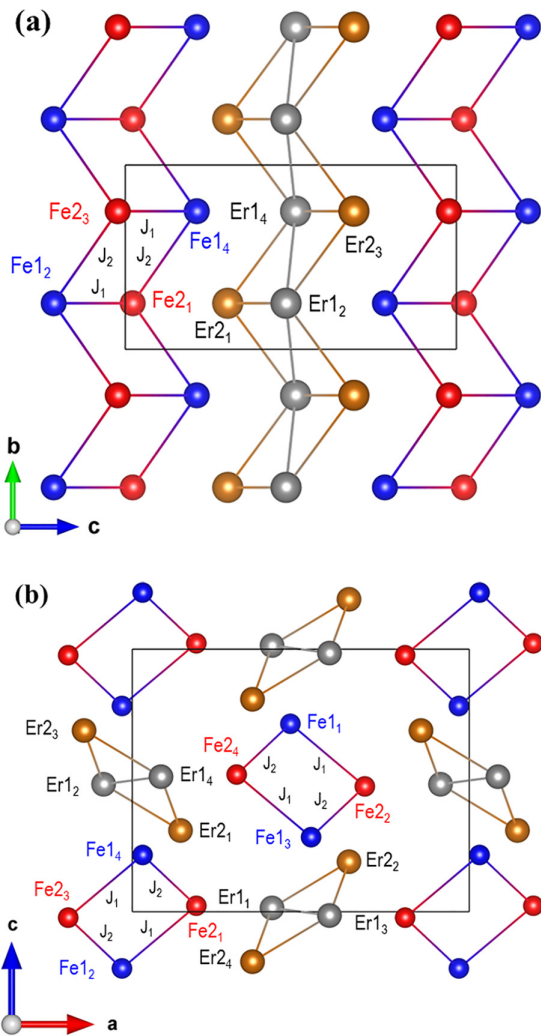


FIG. 1. Arrangement of magnetic Fe³⁺ and Er³⁺ ions in the crystal structure of BaErFeO₄ shown as a projection onto (a) the bc plane and (b) the ac plane. Drawings were made using VESTA [23].

at T_{N2} , in agreement with results for BaDyFeO₄ [7]; on the other hand, no specific heat anomaly was detected at T_{N2} in BaYFeO₄ [7] and BaHoFeO₄ [9]. A very strong specific heat anomaly appeared at T_{N3} , in agreement with results for BaRFeO₄ with magnetic rare-earth elements [7,9]. However, small magnetic fields, as small as 2 kOe, completely suppressed the specific heat anomaly at T_{N2} in BaErFeO₄ (inset of Fig. 4) and also slightly suppressed the anomaly at T_{N3} (Fig. 5). With the increase of an applied magnetic field, the anomaly at T_{N3} continued to be suppressed, and an effect of a large magnetic field (90 kOe) on specific heat was observed far above T_{N1} up to ~ 120 K. It means that a large portion of low-temperature magnetic entropy (observed below ~ 14 K) moved to a high-temperature region.

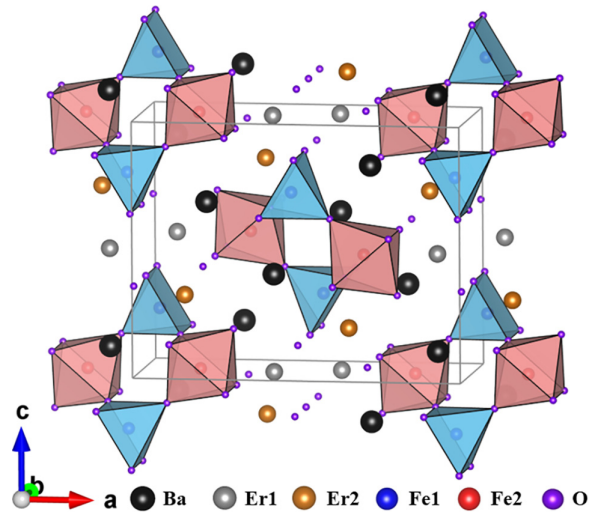


FIG. 2. Orthorhombic crystal structure of BaErFeO₄ consisting of corner-shared units of [FeO₅]⁷⁻ square pyramids (Fe1, blue) and [FeO₆]⁹⁻ octahedra (Fe2, red). The drawing was made using VESTA [23].

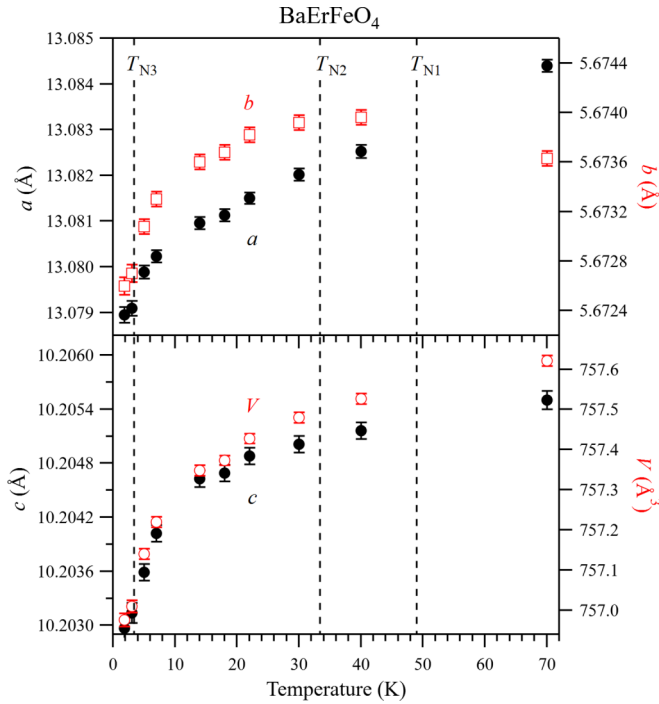


FIG. 3. Temperature dependence of the lattice constants a , b , and c and the volume V of BaErFeO_4 below $T = 70$ K based on neutron diffraction data.

Magnetic susceptibility data showed that the behavior of BaErFeO_4 strongly depended on the measurement magnetic field especially below ~ 10 K (Fig. 6), where a noticeable FM-like contribution appeared above about $H = 1.5$ kOe, and the transition moved to higher temperatures. Here, T_{N1} remained almost unaffected by magnetic fields, while T_{N2} slightly decreased with the increase of a magnetic field. The magnetic susceptibility curves exhibited strong decreases near T_{N2} and T_{N3} below about $H = 1$ kOe, which are unique in the series of BaRFeO_4 ($R = \text{Dy} - \text{Yb}, \text{Y}$) compounds [7,12,11,15] and

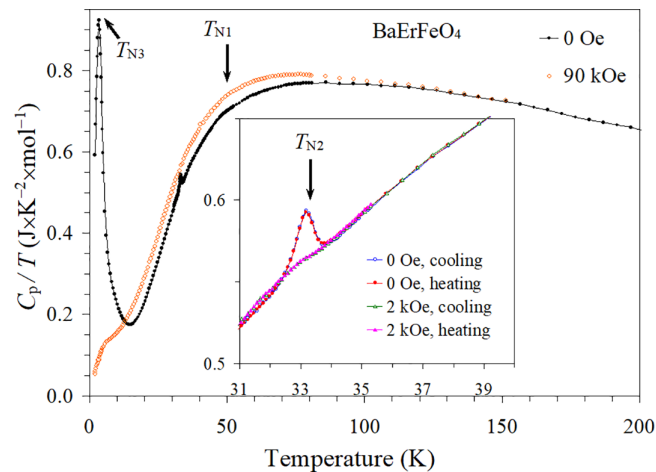


FIG. 4. Specific heat of BaErFeO_4 as C_p/T vs T at 0 Oe (black filled circles with line) and 90 kOe (red empty circles without line), measured on cooling. The inset shows zoomed parts of the C_p/T vs T curves at 0 Oe and 2 kOe on cooling and heating.

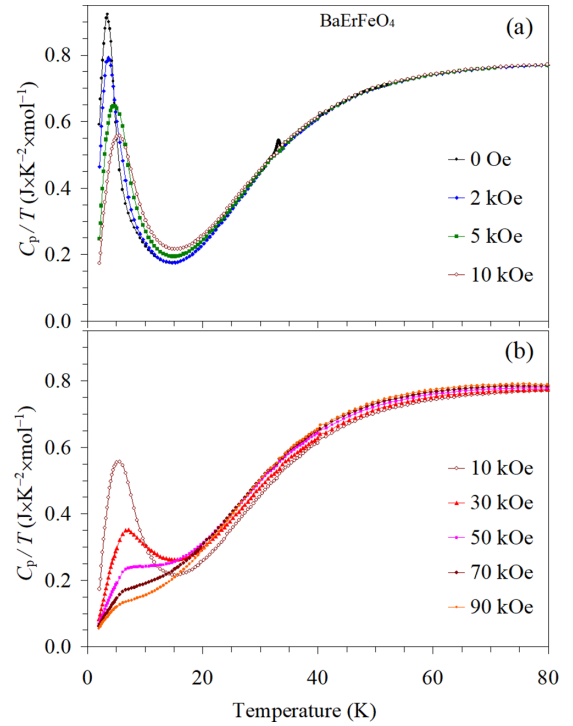


FIG. 5. Specific heat of BaErFeO_4 as C_p/T vs T below 80 K at different magnetic fields, measured on cooling. (a) $H = 0, 2, 5,$ and 10 kOe and (b) $H = 10, 30, 50, 70,$ and 90 kOe.

indicated that the (zero field) magnetic structures of $R = \text{Er}$ are partly different from the previously investigated materials with $R = \text{Yb}, \text{Tm}, \text{Y}$ [12,17]. The complex magnetic behavior of BaErFeO_4 is illustrated in Fig. S1 in the Supplemental Material [24], where magnetic susceptibility data at $H = 1.5$ kOe are plotted in different presentations as an example. The χ^{-1} vs T curve (field-cooled on cooling, 10 kOe) of BaErFeO_4 shown in Fig. 7 could be well fitted by the Curie-Weiss law at high temperatures between 250 and 395 K. However, a noticeable deviation from the Curie-Weiss law is observed below ~ 150 K, that is, far above T_{N1} . The experimental effective magnetic moment $\mu_{\text{eff}} = 10.267(12) \mu_B$

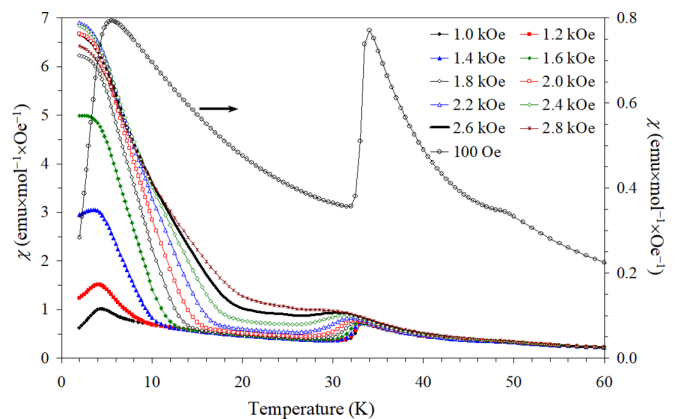


FIG. 6. Magnetic susceptibility curves, χ vs T , of BaErFeO_4 at different magnetic fields from 1.0 to 2.8 kOe with a step of 0.2 kOe (left-hand axis) and at 100 Oe (right-hand axis), measured on cooling.

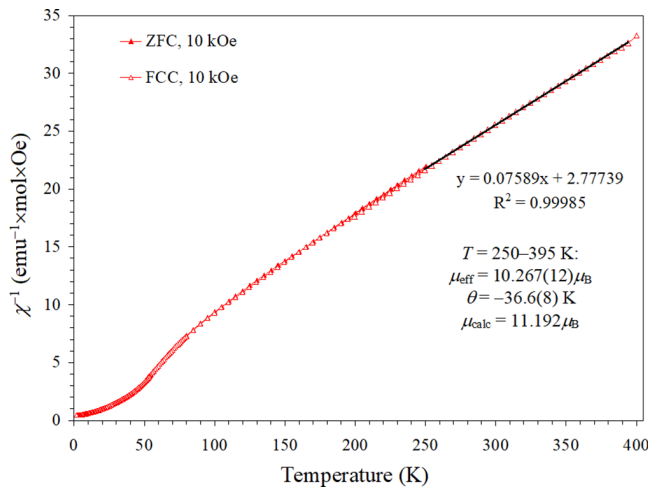


FIG. 7. χ^{-1} vs T curves [zero-field-cooling (ZFC) and field-cooled on cooling (FCC), 10 kOe] of BaErFeO₄ with a Curie-Weiss fit (black line) in the temperature range between 250 and 395 K. Obtained fitting parameters are given in the figure.

is found to be $\sim 8\%$ smaller than the calculated one $\mu_{\text{calc}} = 11.192 \mu_{\text{B}}$. A similar tendency was observed in BaDyFeO₄ ($\mu_{\text{eff}} = 11.28 \mu_{\text{B}}$ vs $\mu_{\text{calc}} = 12.14 \mu_{\text{B}}$) [7]. The Weiss temperature $\theta = -36.6(8)$ K in BaErFeO₄ is close to that of BaDyFeO₄ ($\theta = -34$ K) [7] and BaHoFeO₄ ($\theta = -30$ K) [10]. We note that the Curie-Weiss parameters in BaRFeO₄ could be affected by the presence of impurities with high transition temperatures.

Therefore, both specific heat (at zero magnetic field) and magnetic susceptibility data revealed the presence of three magnetic phase transitions in BaErFeO₄ at $T_{\text{N}1} = 49$ K, $T_{\text{N}2} = 33.4$ K, and $T_{\text{N}3} = 3.4$ K (the temperatures are given at zero or very small magnetic fields). The results of our (zero field) neutron diffraction measurements, described below, confirmed the presence of three magnetic phase transitions at $T_{\text{N}1}$, $T_{\text{N}2}$, and $T_{\text{N}3}$ in BaErFeO₄ with an incommensurate magnetic structure below $T_{\text{N}1}$ and commensurate magnetic structures below $T_{\text{N}2}$.

C. Magnetic structures of BaErFeO₄

Figure 8 shows the refinement of neutron diffraction patterns of BaErFeO₄ measured in the magnetically ordered states at (a) $T = 40$ K (between $T_{\text{N}1}$ and $T_{\text{N}2}$), (b) $T = 22$ K (between $T_{\text{N}2}$ and $T_{\text{N}3}$), and (c) $T = 1.8$ K (below $T_{\text{N}3}$). Simultaneous refinements of crystal and magnetic structures were performed in the full range of scattering angles 2θ up to 162° . The refinements in the full 2θ range are shown in Fig. S2 in the Supplemental Material [24]. The inset of Fig. 8 compares observed neutron intensities measured in the paramagnetic state at $T = 70$ K, the incommensurate phase at $T = 40$ K, and the commensurate phase at $T = 22$ K.

For space group is $Pnma$ (No. 62), the list of all possible magnetic propagation vectors (\mathbf{k}) with different symmetry and the corresponding complex irreducible representations (irreps) are tabulated in Ref. [22] and summarized in Table S1 in the Supplemental Material [24]. To solve the magnetic structures of BaErFeO₄, we have systematically checked

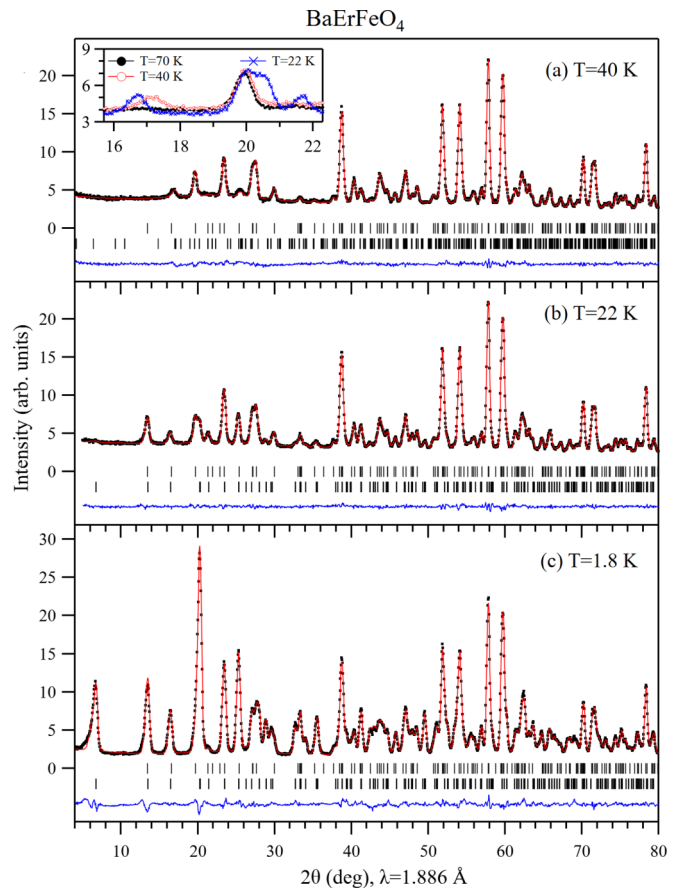


FIG. 8. Experimental (black dots), calculated (red line), and difference (blue line) neutron diffraction patterns of BaErFeO₄ in the magnetically ordered state at (a) $T = 40$ K, (b) $T = 22$ K, and (c) $T = 1.8$ K. Tick marks indicate Bragg peak positions. The first row is for the nuclear peaks, and the second row is for the magnetic peaks. The inset compares observed neutron intensities measured at $T = 70$, 40, and 22 K.

which of the commensurate and incommensurate magnetic propagation vectors from this list can explain peak positions of the experimentally observed magnetic Bragg peaks.

At $T = 40$ K, all magnetic Bragg peaks of BaErFeO₄ can be indexed with an incommensurate propagation vector $\mathbf{k}_1 = (0, 0, k_z)$. Magnetic $3d$ - $3d$ exchange interactions induced magnetic order at the Fe³⁺ ions, and Er³⁺ ions remain disordered. For the space group $Pnma$, site (4c) and the propagation vector \mathbf{k}_1 , representation analysis for the possible magnetic structures gives the result summarized in Table II. There are four irreps, $m\text{LD}1$, $m\text{LD}2$, $m\text{LD}3$, and $m\text{LD}4$, with different symmetry, and the basis vectors are complex. Among the four magnetic ions on site 4c (e.g., Fe₁₄, Fe₁₁, Fe₁₂, and Fe₁₃), only the pairs separated by $\Delta z = \frac{1}{2}$ are coupled by symmetry (e.g., Fe₁₄ with Fe₁₁ and Fe₁₂ with Fe₁₃). The result of the refinement of the magnetic structure at $T = 40$ K is given in Table III. The incommensurate magnetic structure of BaErFeO₄ at $T = 40$ K corresponds to the irrep $m\text{LD}4$ like that in BaYbFeO₄ at $T = 42$ K. Details of the refinement for BaYbFeO₄ are described in Ref. [17]. For BaErFeO₄ at $T = 40$ K, the propagation vector is $\mathbf{k}_1 = (0, 0, k_z)$, with $k_z = 0.396(3)$ and ordered Fe moments of $m_y = 2.50(9) \mu_{\text{B}}$

TABLE II. Group theory analysis for the magnetic structure of BaErFeO₄ between T_{N1} and T_{N2} calculated using ISODISTORT [22] and BASIREPS [20]. The crystallographic space group is $Pnma$ (No. 62). The magnetic propagation vector is $\mathbf{k}_1 = (0, 0, k_z)$. $a = \exp(i\pi k_z)$. $a^* = \exp(-i\pi k_z)$. All magnetic ions (Fe) are located on $4c$ sites, and the positions are shown in Fig. 1(b). Components of the magnetic moments are expressed using (u_1, v_1, w_1) and (u_2, v_2, w_2) in orbits 1 and 2, respectively. Irrep denotes irreducible representation. The character sets correspond to the four symmetry elements [20].^a

irrep (ISODISTORT)	irrep (BASIREPS)	Orbit 1 (x, y, z)	Orbit 1 ($-x + \frac{1}{2}, -y, z + \frac{1}{2}$)	Orbit 2 ($-x, y + \frac{1}{2}, -z$)	Orbit 2 ($x + \frac{1}{2}, -y + \frac{1}{2}, -z + \frac{1}{2}$)
<i>mLD1</i>	IRrep(1)	(0, v_1 , 0)	(0, $-v_1$, 0) · a^*	(0, v_2 , 0)	(0, $-v_2$, 0) · a^*
<i>mLD2</i>	IRrep(2)	(u_1 , 0, w_1)	($-u_1$, 0, w_1) · a^*	(u_2 , 0, w_2)	($-u_2$, 0, w_2) · a^*
<i>mLD3</i>	IRrep(4)	(u_1 , 0, w_1)	(u_1 , 0, $-w_1$) · a^*	(u_2 , 0, w_2)	(u_2 , 0, $-w_2$) · a^*
<i>mLD4</i>	IRrep(3)	(0, v_1 , 0)	(0, v_1 , 0) · a^*	(0, v_2 , 0)	(0, v_2 , 0) · a^*
		Fe1 ₄	Fe1 ₁	Fe1 ₂	Fe1 ₃
		Fe2 ₁	Fe2 ₄	Fe2 ₃	Fe2 ₂

^aPositions of magnetic ions: Fe1₄ (0.032, 0.75, 0.216); Fe1₁ (0.468, 0.25, 0.716); Fe1₂ (−0.032, 0.25, −0.216); Fe1₃ (0.532, 0.75, 0.284); Fe2₁ (0.190, 0.25, 0.023); Fe2₄ (0.310, 0.75, 0.523); Fe2₃ (−0.190, 0.75, −0.023); Fe2₂ (0.690, 0.25, 0.477). Symmetry elements: Symm(1): 1; Symm(2): 2 (0, 0, $\frac{1}{2}$) $\frac{1}{4}$, 0, z ; Symm(3): m x , $\frac{1}{4}$, z ; Symm(4): n (0, $\frac{1}{2}$, $\frac{1}{2}$) $\frac{1}{4}$, y , z . Character sets: *mLD1* (1, a , 1, a); *mLD2* (1, a , −1, − a); *mLD3* (1, − a , −1, a); *mLD4* (1, − a , 1, − a).

are oriented along the b direction, perpendicular to \mathbf{k}_1 . The collinear incommensurate magnetic structure is illustrated in Fig. 9(a). It is a spin density wave (SDW). The size of the ordered moments and the magnetic phase is constant within each ring and chain of Fe³⁺ ions. Nearest-neighbor and second-nearest-neighbor Fe³⁺ ions [see J_1 and J_2 in Fig. 1(b)] are coupled AFM. Along the c direction, the size of ordered Fe moments changes according to the k_z component of the propagation vector \mathbf{k}_1 . Between T_{N1} and T_{N2} , we performed neutron diffraction measurements at two temperatures $T = 40$ and 36 K. The refinement of the magnetic structure at $T = 36$ K, closer to $T_{N2} = 33.4$ K, yielded $k_z = 0.396(3)$, $m_y = 2.70(9) \mu_B$. The temperature dependence of the magnetic propagation vector is very weak (zero within experimental accuracy) with the value $k_z = 0.396(3)$ remaining far away from, for example, $k_z = 0.5$. The ordered Fe moment m_y slightly increased toward lower temperature. Between T_{N1}

and T_{N2} , our results for BaErFeO₄ agree with a more detailed investigation [12] of the temperature dependence of the incommensurate magnetic structure of BaYFeO₄. Magnetic ordering of Mn³⁺ ions in perovskite TmMnO₃ [25] is an example, where below $T_{N1} = 42$ K, the magnetic propagation vector $\mathbf{k}_1 = (k_x, 0, 0)$ exhibits a strong temperature dependence ($0.45 < k_x \leq 0.5$) toward a commensurate structure below $T_{N2} = 32$ K with $\mathbf{k}_2 = (\frac{1}{2}, 0, 0)$.

At $T = 22$ and 1.8 K (below T_{N2}), all magnetic Bragg peaks of BaErFeO₄ can be indexed with a commensurate propagation vector $\mathbf{k}_2 = (\frac{1}{2}, 0, \frac{1}{2})$. As illustrated in Fig. S3 in the Supplemental Material [24], experimental data disagree with the positions of magnetic Bragg peaks for the propagation vectors $\mathbf{k} = (0, 0, \frac{1}{2})$ and $\mathbf{k} = (0, 0, k_z)$. Below T_{N2} , all magnetic Fe³⁺ and Er³⁺ ions are ordered. For the space group $Pnma$, site ($4c$) and the propagation vector \mathbf{k}_2 , represen-

TABLE III. Result of the refinement of the magnetic structures of BaErFeO₄ at $T = 40, 22$, and 1.8 K based on powder neutron diffraction data (HRPT, $\lambda = 1.886$ Å, $\mu R = 0.8$). Positions of the magnetic ions (Fe³⁺, Er³⁺) are labeled as shown in Fig. 1(b). Magnetic phases δ_0 , δ_{Fe} , δ_{Er21} , and δ_{Er14} are in units of 2π .^a

$T = 40$ K ($T_{N2} < T < T_{N1}$): $\mathbf{k}_1 = (0, 0, k_z)$; irrep: <i>mLD4</i> $k_z = 0.396(3)$; $\delta_0 = 0$ Fe1 ₄ : (0, v_1 , 0) δ_0 ; $v_1 = 2.50(9) \mu_B$; Fe1 ₂ : (0, v_2 , 0) δ_0 ; $v_2 = 2.50(9) \mu_B$; Fe2 ₁ : (0, v_1 , 0) δ_0 ; $v_1 = -2.50(9) \mu_B$; Fe2 ₃ : (0, v_2 , 0) δ_0 ; $v_2 = -2.50(9) \mu_B$; $\chi^2 = 2.13$; $R_{wp} = 3.10\%$; $R_{exp} = 2.12\%$; $R_{Bragg} = 2.29\%$; $R_{mag} = 24.7\%$
$T = 22$ K ($T < T_{N2}$): $\mathbf{k}_2 = (\frac{1}{2}, 0, \frac{1}{2})$; irrep: <i>mU2+</i> $\delta_{Fe} = 0.125$; $\delta_{Er21} = -0.235(7)$; $\delta_{Er14} = 0.053(6)$ Fe1 ₄ : (u , 0, w) δ_{Fe} ; $u = -2.20(5) \mu_B$; $w = 2.22(7) \mu_B$; Er1 ₄ : (u , 0, w) δ_{Er14} ; $u = 2.63(6) \mu_B$; $w = -0.42(10) \mu_B$; Fe2 ₁ : (u , 0, w) δ_{Fe} ; $u = 2.20(5) \mu_B$; $w = -2.22(7) \mu_B$; Er2 ₁ : (u , 0, w) δ_{Er21} ; $u = -0.45(7) \mu_B$; $w = 2.32(8) \mu_B$; $\chi^2 = 1.87$; $R_{wp} = 2.85\%$; $R_{exp} = 2.09\%$; $R_{Bragg} = 1.71\%$; $R_{mag} = 3.97\%$
$T = 1.8$ K ($T < T_{N3}$): $\mathbf{k}_2 = (\frac{1}{2}, 0, \frac{1}{2})$; irrep: <i>mU2+</i> $\delta_{Fe} = 0.125$; $\delta_{Er21} = -0.107(2)$; $\delta_{Er14} = -0.106(2)$ Fe1 ₄ : (u , 0, w) δ_{Fe} ; $u = -2.13(4) \mu_B$; $w = 3.16(5) \mu_B$; Er1 ₄ : (u , 0, w) δ_{Er14} ; $u = 8.14(5) \mu_B$; $w = -2.38(6) \mu_B$; Fe2 ₁ : (u , 0, w) δ_{Fe} ; $u = 2.13(4) \mu_B$; $w = -3.16(5) \mu_B$; Er2 ₁ : (u , 0, w) δ_{Er21} ; $u = -1.08(4) \mu_B$; $w = 7.62(5) \mu_B$; $\chi^2 = 4.31$; $R_{wp} = 4.40\%$; $R_{exp} = 2.12\%$; $R_{Bragg} = 2.45\%$; $R_{mag} = 3.46\%$

^aPositions of magnetic ions: Fe1₄ (0.032, 0.75, 0.216); Fe1₂ (−0.032, 0.25, −0.216); Fe2₁ (0.190, 0.25, 0.023); Fe2₃ (−0.190, 0.75, −0.023); Er2₁ (0.143, 0.25, 0.310); Er1₄ (0.085, 0.75, 0.514).

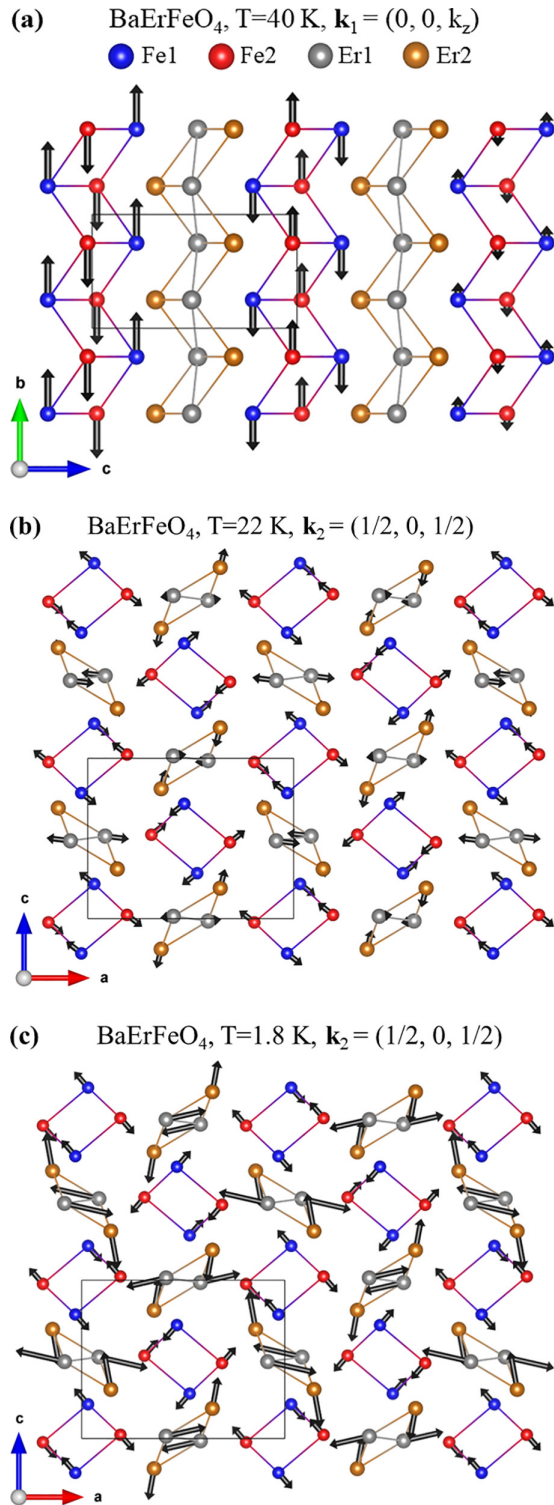


FIG. 9. Illustration of the magnetic structures of BaErFeO₄ at (a) $T = 40$ K, (b) $T = 22$ K, and (c) $T = 1.8$ K. Drawings were made using VESTA [23].

tation analysis for the possible magnetic structures gives the result summarized in Table IV. There are eight irreps, $mU1+$, $mU1-$, $mU2+$, $mU2-$, $mU3+$, $mU3-$, $mU4+$, and $mU4-$, with different symmetry and the basis vectors are complex. All four magnetic ions on site 4c (e.g., Fe₁₄, Fe₁₂, Fe₁₁, and

Fe₁₃) are coupled by symmetry. The result of the refinement of the magnetic structures at $T = 22$ and 1.8 K is given in Table III. The commensurate magnetic structures of BaErFeO₄ at $T = 22$ and 1.8 K correspond to the irrep $mU2+$ and all magnetic ions Fe1, Fe2, Er1, and Er2 are ordered within the ac plane. The commensurate magnetic structures at $T = 22$ and 1.8 K are illustrated in Figs. 9(b) and 9(c), respectively.

For the propagation vector $\mathbf{k}_2 = (\frac{1}{2}, 0, \frac{1}{2})$, the magnetic Fe and Er ions with the positions indicated in Fig. 1(b) are connected by the symmetry operations of site (4c) given in Table IV. For $mU2+$, there is a FM coupling between the ordered moments at (x, y, z) and $(-x, y + \frac{1}{2}, -z)$ as well as between $(-x + \frac{1}{2}, -y, z + \frac{1}{2})$ and $(x + \frac{1}{2}, -y + \frac{1}{2}, -z + \frac{1}{2})$. The first two symmetry operations transform Fe₁₄ into Fe₁₂ inside the same ring shown in Fig. 1(b). The symmetry operations connect all Fe1 and all Fe2 ions with positions indicated in Fig. 1(b) without translations by a lattice constant a or c . (Translations along b can be ignored because of the FM coupling of \mathbf{k}_2 along the b direction.) As a result, for $mU2+$, there is a FM coupling inside each ring for all Fe1 ions as well as for all Fe2 ions. However, this is not true for the positions of Er1 and Er2 ions. The first two symmetry operations transform Er₁₄ into Er_{12-c}. For \mathbf{k}_2 , a translation by the lattice constant c reverses the direction of the ordered Er moment. As a result, for $mU2+$, there is an AFM coupling inside each ring for all Er1 ions as well as for all Er2 ions.

At T_{N2} , a first-order phase transition from an incommensurate magnetic propagation vector $\mathbf{k}_1 = (0, 0, k_z)$ to a commensurate propagation vector $\mathbf{k}_2 = (\frac{1}{2}, 0, \frac{1}{2})$ occurs in BaErFeO₄. All ordered Fe moments change the direction from along the b direction (above T_{N2}) to inside the ac plane (below T_{N2}). Above T_{N2} , the size of ordered Fe moments changes between different chains along the c direction. Below T_{N2} , the size of all ordered Fe1 and Fe2 moments is constant with a noncollinear coupling between different chains along the $[1, 0, 1]$ direction. All Fe moments are approximately parallel or antiparallel to $[1, 0, 1]$ or $[1, 0, -1]$ directions [see Figs. 9(b) and 9(c)]. The temperature dependence of the magnetic phase and the ordered Fe moments below T_{N2} is shown in Fig. 10 in blue color. The magnetic phase $\delta_{Fe} = 0.125$ is equal for all Fe1 and Fe2 ions and temperature independent [Fig. 10(a)]. The temperature dependence of the ordered Fe moment is weak [Fig. 10(c)] and slightly increases from $2.21(6) \mu_B$ at $T = 22$ K to $2.70(4) \mu_B$ at $T = 1.8$ K (Table V) due to a small increase of the m_z component below $T \approx 12$ K [Fig. 11(a)].

Magnetic Er³⁺ ions order at the first-order phase transition at $T_{N2} = 33.4$ K. At $T = 22$ K, $3d-4f$ exchange interactions induced a strongly noncollinear structure with an ordered moment of $2.52(11) \mu_B$ predominantly along the a direction at Er₁₄ and Er₁₂ and an ordered moment of $2.36(11) \mu_B$ predominantly along the c direction at Er₂₂ and Er₂₄ [see Figs. 9(b) and 1(b) and Table V]. In contrast, the ordered moments at Er₁₁, Er₁₃, Er₂₁, and Er₂₃ are much smaller and close to zero. For \mathbf{k}_2 , all Er1 and Er2 ions are coupled by symmetry. Within each ring of Er ions [Fig. 1(b)], the ordered Er moments and the magnetic phases are not constant (Fig. 10, Table III), resulting in a large magnetic phase difference between Er₁₄ and Er₂₁ of 0.29(1).

TABLE IV. Group theory analysis for the magnetic structure of BaErFeO₄ below T_{N2} calculated using ISODISTORT [22] and BASIREPS [20]. The crystallographic space group is $Pnma$ (No. 62). The magnetic propagation vector is $\mathbf{k}_2 = (\frac{1}{2}, 0, \frac{1}{2})$. All magnetic ions (Fe, Er) are located on $4c$ sites, and the location is shown in Fig. 1(b). The components of the magnetic moments are expressed using (u, v, w) . irrep denotes irreducible representation. The character sets correspond to the eight symmetry elements [20].^a

irrep (ISODISTORT)	irrep (BASIREPS)	(x, y, z)	$(-x, y + \frac{1}{2}, -z)$	$(-x + \frac{1}{2}, -y, z + \frac{1}{2})$	$(x + \frac{1}{2}, -y + \frac{1}{2}, -z + \frac{1}{2})$
$mU1+$	IRrep(1)	$(0, v, 0)$	$(0, v, 0)$	$(0, v, 0) \cdot i$	$(0, v, 0) \cdot i$
$mU1-$	IRrep(2)	$(u, 0, w)$	$(-u, 0, -w)$	$(u, 0, -w) \cdot i$	$(-u, 0, w) \cdot i$
$mU2+$	IRrep(3)	$(u, 0, w)$	$(u, 0, w)$	$(u, 0, -w) \cdot i$	$(u, 0, -w) \cdot i$
$mU2-$	IRrep(4)	$(0, v, 0)$	$(0, -v, 0)$	$(0, v, 0) \cdot i$	$(0, -v, 0) \cdot i$
$mU3+$	IRrep(7)	$(u, 0, w)$	$(u, 0, w)$	$(-u, 0, w) \cdot i$	$(-u, 0, w) \cdot i$
$mU3-$	IRrep(8)	$(0, v, 0)$	$(0, -v, 0)$	$(0, -v, 0) \cdot i$	$(0, v, 0) \cdot i$
$mU4+$	IRrep(5)	$(0, v, 0)$	$(0, v, 0)$	$(0, -v, 0) \cdot i$	$(0, -v, 0) \cdot i$
$mU4-$	IRrep(6)	$(u, 0, w)$	$(-u, 0, -w)$	$(-u, 0, w) \cdot i$	$(u, 0, -w) \cdot i$
		Fe1 ₄	Fe1 ₂	Fe1 ₁	Fe1 ₃
		Fe2 ₁	Fe2 ₃	Fe2 ₄	Fe2 ₂
		Er1 ₄	Er1 ₂ - c	Er1 ₁ + c	Er1 ₃
		Er2 ₁	Er2 ₃ - c	Er2 ₄ + c	Er2 ₂

^aPositions of magnetic ions: Fe1₄ (0.032, 0.75, 0.216); Fe1₂ (-0.032, 0.25, -0.216); Fe1₁ (0.468, 0.25, 0.716); Fe1₃ (0.532, 0.75, 0.284); Fe2₁ (0.190, 0.25, 0.023); Fe2₃ (-0.190, 0.75, -0.023); Fe2₄ (0.310, 0.75, 0.523); Fe2₂ (0.690, 0.25, 0.477); Er1₄ (0.085, 0.75, 0.514); Er1₂ (-0.085, 0.25, 0.486); Er1₁ (0.415, 0.25, 0.014); Er1₃ (0.585, 0.75, -0.014); Er2₁ (0.143, 0.25, 0.310); Er2₃ (-0.143, 0.75, 0.690); Er2₂ (0.357, 0.75, -0.190); Er2₄ (0.643, 0.25, 0.190). Symmetry elements: Symm(1): 1; Symm(2): $2(0, 0, \frac{1}{2}) \frac{1}{4}, 0, z$; Symm(3): $2(0, \frac{1}{2}, 0) 0, y, 0$; Symm(4): $2(\frac{1}{2}, 0, 0) x, \frac{1}{4}, \frac{1}{4}$; Symm(5): $-1 0, 0, 0$; Symm(6): $a x, y, \frac{1}{4}$; Symm(7): $m x, \frac{1}{4}, z$; Symm(8): $n(0, \frac{1}{2}, \frac{1}{2}) \frac{1}{4}, y, z$. Character sets: $mU1+$ (1, $i, 1, i, 1, i, 1, i$); $mU1-$ (1, $i, 1, i, -1, -i, -1, -i$); $mU2+$ (1, $i, -1, -i, 1, i, -1, -i$); $mU2-$ (1, $i, -1, -i, -1, -i, -1, i$); $mU3+$ (1, $-i, -1, i, 1, -i, -1, i$); $mU3-$ (1, $-i, -1, i, -1, i, 1, -i$); $mU4+$ (1, $-i, 1, -i, 1, -i, 1, -i$); $mU4-$ (1, $-i, 1, -i, -1, i, -1, i$).

With decreasing temperature, the specific heat C_p/T starts to increase below ~ 12 K toward a strong peak at $T_{N3} = 3.4$ K (Fig. 4). The magnetic entropy of this C_p/T peak corresponds to a change of the magnetic structure induced by $4f$ - $4f$ exchange interactions. Inside each ring of Er ions, the large magnetic phase difference becomes smaller and reaches zero at T_{N3} [Figs. 10(a) and 10(b)]. At the same time, the small ordered Er moments start to increase [Fig. 10(c)]. At $T = 1.8$ K, all ordered Er moments have large values between 4.8 and 6.7 μ_B (Table V). Below T_{N3} , Er ions in the same ring have a constant magnetic phase (like the Fe ions), but the magnetic structure is noncollinear (different from the Fe ions). The temperature dependence of the ordered Er moments and the components (m_x, m_z) is shown in Figs. 10 and 11, respectively. As shown in Fig. 10(a), at $T = 22$ K, the magnetic phases of $\delta(\text{Er}1_4)$ and $\delta(\text{Er}2_1)$ have different signs of positive and negative, respectively. Toward the zero-phase difference at T_{N3} , the sign of $\delta(\text{Er}1_4)$ changes from positive to negative near 7 K, where the ordered moments of Er1₁ and Er1₃ exhibit a minimum of zero [Fig. 10(c)]. This minimum is caused by a reversal of the direction of both components m_x and m_z , as shown in Fig. 11(c) for Er1₁. Such a minimum is not observed for Er2 because the magnetic phase $\delta(\text{Er}2_1)$ remains negative [Fig. 10(a)] between 1.8 and 30 K.

We checked the effect of absorption (for $0.0 \leq \mu R \leq 2.0$) on the refined magnetic structures given in Table III. Correlations with the ordered moments and phase factors were found to be very weak (values within the errors given in Table III). As a conclusion, the Er absorption can be neglected in our magnetic structure refinements.

The Thompson-Cox-Hastings pseudo-Voigt function used in the refinement of the neutron data consists of a Gaussian and a Lorentzian component. The correlation lengths (L)

of the magnetic and the crystal structure can be compared from the Lorentzian peak broadening of the resolution parameter Y (Y_m and Y_n for the magnetic and crystal structure, respectively). From the refinement of the crystal structure in the paramagnetic state at $T = 70$ K, we obtained $Y_n = 0.0487(18)$. This value of Y_n was kept fixed for the refinements of the magnetic structures. We assume that the Lorentzian size effect contribution to the width of nuclear peaks is resolution limited because the Y_n parameter of the Cagliotti function [20,26] is close to the instrumental value. The microstrain contribution given by the resolution parameter U of the Gaussian component was fixed by nuclear peaks for the magnetic peaks. In the incommensurate phase at $T = 40$ K, a large Lorentzian peak broadening with $Y_m = 0.36(6)$ or $Y_m/Y_n = 7.4(1.3)$ indicates a magnetic structure with a much shorter correlation length. Using the well-known Debye-Scherrer formula $\sigma_1 = Y_m - Y_n = \lambda/L$ [27], where $\lambda = 1.886$ Å is the neutron wavelength, the correlation length of the magnetic structure at $T = 40$ K can be estimated as $L = 350(70)$ Å. In the commensurate phase, the Lorentzian peak broadening is much smaller with $Y_m = 0.070(9)$ or $Y_m/Y_n = 1.4(2)$ at $T = 22$ K and $Y_m = 0.055(3)$ or $Y_m/Y_n = 1.1(1)$ at $T = 1.8$ K. Compared with the crystal structure, the correlation length of the magnetic structure is only slightly shorter at $T = 22$ K and almost equal at $T = 1.8$ K. At T_{N2} , the magnetic susceptibility at zero field exhibits a large steep decrease (Fig. 6) and the correlation length of the magnetic structure shows a large increase between the incommensurate ($T = 40$ K) and the commensurate structure ($T = 22$ K). At T_{N3} , the magnetic susceptibility exhibits another large steep decrease (Fig. 6), and the correlation length of the magnetic structure increases from a slightly shorter ($T = 22$ K) to an almost equal value ($T = 1.8$ K) compared with that of the crystal structure.

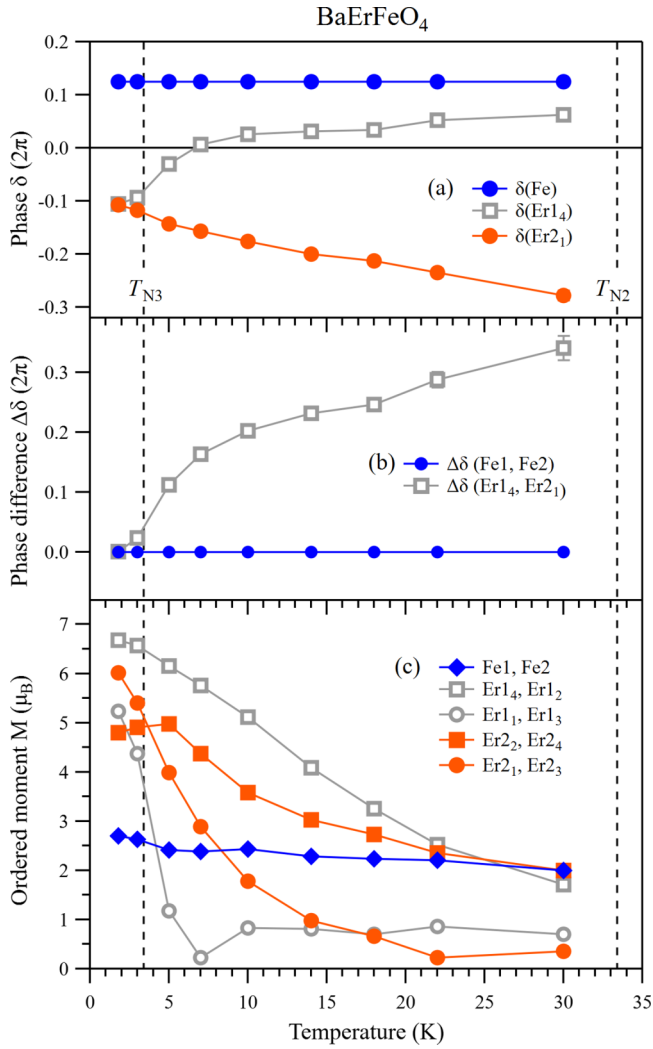


FIG. 10. Temperature dependence of (a) the magnetic phase δ , (b) the phase difference $\Delta\delta$, and (c) the ordered magnetic Fe^{3+} and Er^{3+} moments of BaErFeO_4 below T_{N2} . δ and $\Delta\delta$ are given in units of 2π .

TABLE V. Ordered magnetic moments $M(m_x, m_y, m_z)$ in units of μ_B at $T = 40, 22$, and 1.8 K calculated for the rings of BaErFeO_4 . Positions of the magnetic ions (Fe^{3+} , Er^{3+}) are labeled as shown in Fig. 1(b).^a

Ion	$T = 40$ K	$T = 22$ K	$T = 1.8$ K
$\text{Fe}_{14}; \text{Fe}_{12}$	2.50 (0, 2.50, 0)	2.21 (−1.55, 0, 1.57)	2.70 (−1.51, 0, 2.24)
$\text{Fe}_{21}; \text{Fe}_{23}$	2.50 (0, −2.50, 0)	2.21 (1.55, 0, −1.57)	2.70 (1.51, 0, −2.24)
$\text{Fe}_{11}; \text{Fe}_{13}$	2.50 (0, 2.50, 0)	2.21 (−1.55, 0, −1.57)	2.70 (−1.51, 0, −2.24)
$\text{Fe}_{24}; \text{Fe}_{22}$	2.50 (0, −2.50, 0)	2.21 (1.55, 0, 1.57)	2.70 (1.51, 0, 2.24)
$\text{Er}_{14}; -\text{Er}_{12}$	–	2.52 (2.49, 0, −0.40)	6.68 (6.41, 0, −1.87)
$\text{Er}_{21}; -\text{Er}_{23}$	–	0.23 (−0.04, 0, 0.22)	6.02 (−0.85, 0, 5.96)
$\text{Er}_{11}; -\text{Er}_{13}$	–	0.87 (−0.85, 0, −0.14)	5.23 (5.02, 0, 1.47)
$\text{Er}_{22}; -\text{Er}_{24}$	–	2.36 (0.45, 0, 2.31)	4.80 (0.67, 0, 4.75)

^aPositions of magnetic ions: Fe_{14} (0.032, 0.75, 0.216); Fe_{12} (−0.032, 0.25, −0.216); Fe_{11} (0.468, 0.25, 0.716); Fe_{13} (0.532, 0.75, 0.284); Fe_{21} (0.190, 0.25, 0.023); Fe_{23} (−0.190, 0.75, −0.023); Fe_{24} (0.310, 0.75, 0.523); Fe_{22} (0.690, 0.25, 0.477); Er_{14} (0.085, 0.75, 0.514); Er_{12} (−0.085, 0.25, 0.486); Er_{11} (0.415, 0.25, 0.014); Er_{13} (0.585, 0.75, −0.014); Er_{21} (0.143, 0.25, 0.310); Er_{23} (−0.143, 0.75, 0.690); Er_{22} (0.643, 0.25, 0.190); Er_{24} (0.357, 0.75, −0.190). Ordered magnetic moments with errors: (Fe, $T = 40$ K) 2.50(9); (Fe, $T = 22$ K) 2.21(6); 1.55(4); 1.57(5); (Er, $T = 1.8$ K) 2.70(4); 1.51(3); 2.24(4); (Er, $T = 22$ K) 2.52(11); 2.49(6); 0.40(9); 0.23(1); 0.04(1); 0.22(1); 0.87(4); 0.85(2); 0.14(3); 2.36(11); 0.45(7); 2.31(8); (Er, $T = 1.8$ K) 6.68(6); 6.41(4); 1.87(5); 6.02(5); 0.85(4); 5.96(4); 5.23(5); 5.02(3); 1.47(4); 4.80(4); 0.67(3); 4.75(3).

D. Comparison of magnetic structures of BaRFeO_4 compounds

Up to date, the determination of magnetic structures of isostructural BaRFeO_4 ferrite compounds by neutron diffraction has been reported for $R = \text{Yb}$ [17], Tm [17], Er (this paper), and Y [12]. These compounds are compared in Table VI in order of increasing R^{3+} ionic radii. Three successive magnetic phase transitions are observed for the materials with magnetic R^{3+} cations, and two phase transitions for BaYFeO_4 with the nonmagnetic Y^{3+} cation. The BaRFeO_4 compounds with $R = \text{Yb}, \text{Tm}, \text{Y}$, adopt incommensurate magnetic structures below T_{N1} with the propagation vector $\mathbf{k}_1 = (0, 0, k_z)$ being stable down to the lowest measured temperature. A phase transition to a commensurate magnetic structure has not been observed. The BaErFeO_4 compound reported in this paper is the first example in this series where the incommensurate magnetic structure with \mathbf{k}_1 changes at T_{N2} to a commensurate AFM structure with $\mathbf{k}_2 = (\frac{1}{2}, 0, \frac{1}{2})$.

The relative values of the various spin exchange constants of the parent compound BaYFeO_4 were calculated in a theoretical study using extended Hückel spin dimer analysis [11]. The result suggested the presence of strong AFM Fe-Fe spin-exchange coupling between square pyramidal (Fe1) and octahedral (Fe2) centers inside each Fe chain compared with much weaker inter-chain magnetic Fe-Fe exchange interactions. Such a behavior has been experimentally observed for the magnetic structures of BaRFeO_4 ferrites with $R = \text{Yb}, \text{Tm},$ and Y [12,17]. A collinear AFM structure with a constant ordered Fe moment and a constant magnetic phase appears inside each Fe chain for all magnetic structures of these compounds. According to our neutron diffraction results, also BaErFeO_4 shows such a behavior for all magnetic structures (see Fig. 9). Interchain magnetic Fe-Fe exchange interactions along various possible pathways are much weaker and determine the magnetic propagation vector and the choice of the irrep. The different behavior between the BaRFeO_4 compounds reflects the different magnetic anisotropy and size of the magnetic R^{3+} ions. Compared with the ferrite compounds with smaller R^{3+} ions ($R = \text{Yb}, \text{Tm}$), BaErFeO_4 belongs to a different group of magnetic structures. It would be interesting

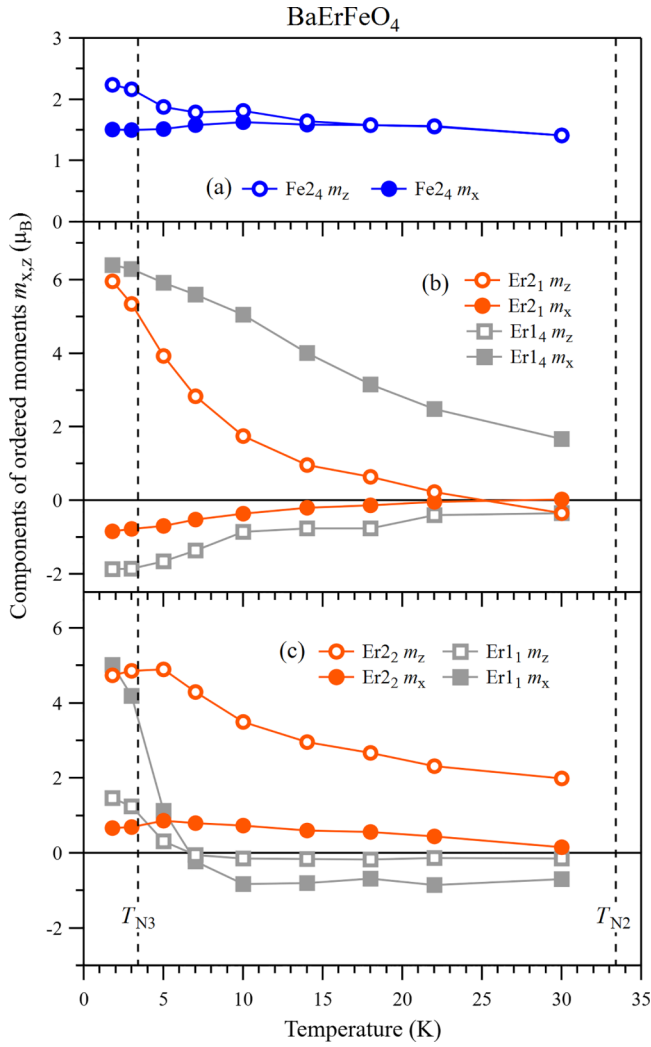


FIG. 11. Temperature dependence of the components of ordered magnetic Fe^{3+} and Er^{3+} moments (m_x, m_z) along the a and c directions of BaErFeO_4 below T_{N2} .

to verify by neutron diffraction whether the commensurate magnetic structure with $\mathbf{k}_2 = (\frac{1}{2}, 0, \frac{1}{2})$ is present in the compounds with larger magnetic R^{3+} ions ($R = \text{Ho}, \text{Dy}$). The ionic radius of Y^{3+} is larger than that of Er^{3+} , but the phase transition has not been observed in BaYFeO_4 , possibly because Y^{3+} is nonmagnetic. We note that the spin dimer calculations [11] predicted for BaYFeO_4 a magnetic structure with $\mathbf{k} = (0, 0, 0)$. Experimentally, such a propagation vector has not been observed in any of the investigated BaRFeO_4 ferrites ($R = \text{Er}, \text{Tm}, \text{Yb}, \text{Y}$).

For all compounds of Table VI, magnetic ordering of Fe^{3+} ions occurs in two successive magnetic phase transitions at T_{N1} and T_{N2} . Below T_{N1} , all compounds adopt a SDW magnetic structure with the same incommensurate propagation vector $\mathbf{k}_1 = (0, 0, k_z)$ and the same irrep $m\text{LD}4$. Ordered Fe moments are oriented along the b direction and rare-earth ions are disordered. For the compounds with $R = \text{Yb}, \text{Tm}$, and Y , the magnetic propagation vector \mathbf{k}_1 is stable at T_{N2} and rare-earth ions remain disordered. For $T < T_{N2}$, ordered Fe moments appear inside the ac plane and coexist with the

b component of the SDW structure ($T_{N2} < T < T_{N1}$). The resulting incommensurate magnetic structures belong to two different irreps and have two order parameters. They correspond to a cycloidal spiral ($R = \text{Yb}, \text{Tm}$) or a cycloid ($R = \text{Y}$). In contrast, for BaErFeO_4 , the change of the magnetic propagation vector to $\mathbf{k}_2 = (\frac{1}{2}, 0, \frac{1}{2})$ at T_{N2} coincides to the onset of magnetic ordering of rare-earth ions. Ordered Fe moments (as well as ordered Er moments) appear inside the ac plane and the b component (of the SDW structure) disappears. The resulting AFM structure belongs to a single irrep with one order parameter. In this sense, the phase transition from \mathbf{k}_1 to \mathbf{k}_2 at T_{N2} in BaErFeO_4 is driven by the appearance of magnetic ordering of Er^{3+} ions through $3d\text{-}4f$ exchange interactions.

The symmetry of the magnetic structures with \mathbf{k}_1 and \mathbf{k}_2 is different. Therefore, below T_{N2} the magnetic structures of BaRFeO_4 compounds with different propagation vectors cannot be compared directly. For the nonmagnetic $R = \text{Y}^{3+}$ ion, the third magnetic phase transition at T_{N3} is absent. For $R = \text{Yb}$ and Tm , with \mathbf{k}_1 , the onset of magnetic order of the rare-earth ions appears at T_{N3} , at much lower temperature than T_{N2} . For $R = \text{Yb}$, $4f\text{-}4f$ exchange interactions produce a collinear AFM structure, where the size and the magnetic phase of ordered Yb moments is constant inside each Yb chain. For $R = \text{Tm}$, $3d\text{-}4f$ coupling induces magnetic order at part of the Tm ions. Ordered Tm2 ions coexist with disordered Tm1 ions due to frustration of magnetic exchange interactions. Inside each Tm chain, both size and the magnetic phase of the ordered Tm moments are not constant. Down to the lowest measured temperature ($T = 1.6$ K), $4f\text{-}4f$ exchange interactions are too weak to produce magnetic order of Tm1 ions in BaTmFeO_4 . For $R = \text{Er}$ with \mathbf{k}_2 , $3d\text{-}4f$ exchange interactions induce magnetic order at T_{N2} . Because of the symmetry of \mathbf{k}_2 , all Er ions order at T_{N2} . Inside each Er chain, both size and magnetic phase of ordered Er moments are not constant close to T_{N2} . With decreasing temperature, the $4f\text{-}4f$ exchange interactions gradually get stronger and modify the magnetic structure of the Er ions. At T_{N3} , each Er chain reached a constant magnetic phase [Fig. 10(a)] and a comparable large size of the Er1 and Er2 ions with a noncollinear arrangement [Figs. 9(c) and 10(c)]. Interestingly, magnetic structures of rare-earth ions stabilized by $3d\text{-}4f$ exchange interactions (observed for BaTmFeO_4 at T_{N3}) and by $4f\text{-}4f$ exchange interactions (observed for BaYbFeO_4 at T_{N3}) both appear in BaErFeO_4 at T_{N2} and T_{N3} , respectively.

IV. SUMMARY

In the orthorhombic crystal structure (space group $Pnma$) of the ferrite compound BaErFeO_4 , magnetic ions (Fe1 and Fe2, as well as Er1 and Er2) form spin chains propagating along the b direction. The lattice geometry supports frustration of magnetic exchange interactions that can lead to complex magnetic structures with multiple phase transitions. Based on macroscopic measurements (specific heat and magnetic susceptibility), we showed that BaErFeO_4 undergoes three successive magnetic phase transitions at $T_{N1} = 49$ K, $T_{N2} = 33.4$ K, and $T_{N3} = 3.4$ K. We employed neutron diffraction to determine the magnetic structures. In this paper, we show that BaErFeO_4 is the first member in the series of the BaRFeO_4 (R : rare earth) ferrite compounds that shows a rare-earth driven

TABLE VI. Comparison of the magnetic structures of BaRFeO_4 , ($R = \text{Yb, Tm, Er, Y}$) compounds in order of increasing ionic R^{3+} ionic radii. Magnetic phase transitions temperatures (T_{N1} , T_{N2} , T_{N3}). Magnetic propagation vectors $\mathbf{k}_1 = (0, 0, k_z)$, $\mathbf{k}_2 = (\frac{1}{2}, 0, \frac{1}{2})$. Irrep: irreducible representation. Maximum (M_{\max}) and minimum (M_{\min}) ordered moment. Ordered components: m_x, m_y, m_z . *: no neutron data available.

	BaYbFeO ₄ [17]	BaTmFeO ₄ [17]	BaErFeO ₄ (this paper)	BaYFeO ₄ [12]
T_{N1}, T_{N2}, T_{N3} (K)	57, 36, ≈ 18	47.5, 46, ≈ 6	49, 33.4, 3.4	48, 36, –
Ordering of Fe^{3+}	$\text{Fe}^{3+}; T_{N2} < T < T_{N1}$	$\text{Fe}^{3+}; T_{N2} < T < T_{N1}$	$\text{Fe}^{3+}; T_{N2} < T < T_{N1}$	$\text{Fe}^{3+}; T_{N2} < T < T_{N1}$
Propagation vector	$\mathbf{k}_1 = (0, 0, k_z)$	$\mathbf{k}_1 = (0, 0, k_z)$	$\mathbf{k}_1 = (0, 0, k_z)$	$\mathbf{k}_1 = (0, 0, k_z)$
irrep	$m\text{LD4}$	$m\text{LD4}$	$m\text{LD4}$	$m\text{LD4}$
Structure type	SDW	SDW	SDW	SDW
$k_z; T$	0.315(1); 42 K	*	0.396(3); 40 K	0.333; 38 K
M_{\max} (μ_B); T	2.70(7); 42 K	*	2.50(9); 40 K	2.2(2); 3.0(2); 38 K
Ordered components	m_y	*	m_y	m_y
Ordering of Fe^{3+}	$\text{Fe}^{3+}; T < T_{N2}$	$\text{Fe}^{3+}; T < T_{N2}$	$\text{Fe}^{3+}; T < T_{N2}$	$\text{Fe}^{3+}; T < T_{N2}$
Propagation vector	$\mathbf{k}_1 = (0, 0, k_z)$	$\mathbf{k}_1 = (0, 0, k_z)$	$\mathbf{k}_2 = (\frac{1}{2}, 0, \frac{1}{2})$	$\mathbf{k}_1 = (0, 0, k_z)$
irrep	$m\text{LD4} + m\text{LD3}$	$m\text{LD4} + m\text{LD2}$	$m\text{U2+}$	$m\text{LD4} + m\text{LD2}$
Structure type	Cycloidal spiral	Cycloidal spiral	Commensurate, AFM	Cycloid
$k_z; T$	0.314(1); 25 K 0.293(2); 1.6 K	0.374(1); 28 K 0.375(1); 1.6 K	–	0.358(2); 6 K
$M_{\max}; M_{\min}$ (μ_B); T	3.96; 2.87; 1.6 K	3.42; 3.06; 1.6 K	2.70; 2.70; 1.8 K	3.0(1); 2.8(1); 6 K
Ordered components	m_x, m_y, m_z	m_x, m_y, m_z	m_x, m_z	m_y, m_z
Ordering of R^{3+}	$\text{Yb}^{3+}; T < T_{N3}$	$\text{Tm}^{3+}; T < T_{N3}$	$\text{Er}^{3+}; T < T_{N2}$	–
Propagation vector	$\mathbf{k}_1 = (0, 0, k_z)$	$\mathbf{k}_1 = (0, 0, k_z)$	$\mathbf{k}_2 = (\frac{1}{2}, 0, \frac{1}{2})$	–
irrep	$m\text{LD3}$	$m\text{LD2}$	$m\text{U2+}$	–
Structure type	SDW	SDW	Commensurate, AFM	–
Stabilized by	$4f\text{-}4f$ ($T < T_{N3}$)	$3d\text{-}4f$ ($T < T_{N3}$)	$3d\text{-}4f$ ($T < T_{N2}$) $4f\text{-}4f$ ($T < T_{N3}$)	–
$k_z; T$	0.293(2); 1.6 K	0.375(1); 1.6 K	–	–
M_{\max} (μ_B); T	2.00(7); 1.6 K	3.20(7); 1.6 K	4.80–6.67; 1.8 K	–
Ordered components	m_x	m_x, m_z	m_x, m_z	–

phase transition from an incommensurate SDW structure with $\mathbf{k}_1 = (0, 0, k_z)$ below T_{N1} to a commensurate AFM structure with $\mathbf{k}_2 = (\frac{1}{2}, 0, \frac{1}{2})$ below T_{N2} . At T_{N1} , $3d\text{-}3d$ exchange interactions produce collinear AFM ordering of Fe^{3+} cations with a constant magnetic phase in each Fe spin chain. At T_{N3} , $4f\text{-}4f$ exchange interactions stabilize noncollinear AFM ordering of Er^{3+} cations with a constant magnetic phase in each Er spin chain. At T_{N2} , $3d\text{-}4f$ exchange coupling induces strongly noncollinear magnetic order at all Er^{3+} cations with a large magnetic phase difference in each Er spin chain. The appearance of magnetic Er^{3+} ordering at T_{N2} coincides with a change of the direction of the Fe^{3+} moments from the b direction (above T_{N2}) to inside the ac plane (below T_{N2}) and a phase transition from \mathbf{k}_1 to \mathbf{k}_2 . For the BaRFeO_4 ferrites with

smaller R^{3+} cations ($R = \text{Tm, Yb}$) and nonmagnetic $R = \text{Y}$, the rare-earth ions remain disordered at T_{N2} and the magnetic structure remains incommensurate with a propagation vector \mathbf{k}_1 . The magnetic susceptibility of BaErFeO_4 shows sharp decreases at T_{N2} and at T_{N3} that coincide with large increases of the correlation length of the magnetic structure. Magnetic properties of BaErFeO_4 are unique in the series of BaRFeO_4 ferrites.

ACKNOWLEDGMENTS

This paper is partially based on experiments performed on HRPT diffractometer (Proposal No. 20202060) at the Swiss Spallation Neutron Source SINQ, Paul Scherrer Institute, Switzerland.

- [1] A. R. Oganov, C. J. Pickard, Q. Zhu, and R. J. Needs, Structure prediction drives materials discovery, *Nat. Rev. Mater* **4**, 331 (2019).
[2] Y. A. Izyumov, V. E. Naish, and R. P. Ozerov, *Neutron Diffraction of Magnetic Materials* (Springer, New York, 1991).
[3] J. M. Perez-Mato, J. L. Ribeiro, V. Petricek, and M. Aroyo, Magnetic superspace groups and symmetry constraints in incommensurate magnetic phases, *J. Phys.: Condens. Matter* **24**, 163201 (2012).

- [4] H. T. Stokes, B. J. Campbell, and R. Cordes, Tabulation of irreducible representations of the crystallographic space groups and their superspace extensions, *Acta Cryst. A* **69**, 388 (2013).
[5] P. Yanda, I. V. Golosovsky, I. Mirebeau, N. V. Ter-Oganessian, J. Rodríguez-Carvajal, and A. Sundaresan, Interplay of $4f\text{-}3d$ interactions and spin-induced ferroelectricity in the green phase $\text{Gd}_2\text{BaCuO}_5$, *Phys. Rev. Res.* **2**, 023271 (2020).
[6] A. Dönni, V. Y. Pomjakushin, L. Zhang, K. Yamaura, and A. A. Belik, Temperature evolution of $3d\text{-}$ and $4f\text{-}$ electron mag-

- netic ordering in the ferrimagnetic Mn self-doped perovskite ($\text{Yb}_{0.667}\text{Mn}_{0.333}\text{MnO}_3$), *J. Phys.: Condens. Matter* **33**, 205804 (2021).
- [7] A. A. Belik, N. Terada, Y. Katsuya, M. Tanaka, I. S. Glazkova, A. V. Sobolev, I. A. Presniakov, and K. Yamaura, Synthesis, structure, and magnetic and dielectric properties of magnetoelectric BaDyFeO_4 ferrite, *J. Alloys Compd.* **811**, 151963 (2019).
- [8] A. A. Belik, A. Dönni, M. Tanaka, I. S. Glazkova, A. V. Sobolev, and I. A. Presniakov, Different magnetic and magnetodielectric behavior of BaRFeO_4 ferrites with $R = \text{Ho}$, Er , Tm , and Yb , *J. Alloys Compd.* **922**, 166297 (2022).
- [9] R. Kumar and A. Sundaresan, Unveiling a hidden multiferroic state under magnetic fields in BaHoFeO_4 , *Phys. Rev. B* **107**, 184420 (2023).
- [10] C. H. Prashanth, T. W. Yen, A. Tiwari, P. Athira, S. M. Huang, B. R. Poojitha, D. P. Gulo, H. L. Liu, C. W. Wang, Y. K. Lin *et al.*, Interplay of magnetic and electric coupling across the spin density wave to conical magnetic ordering in a BaHoFeO_4 spin-cluster chain compound, *J. Alloys Compd.* **942**, 169017 (2023).
- [11] F. Wrobel, M. C. Kemei, and S. Derakhshan, Antiferromagnetic spin correlations between corner-shared $[\text{FeO}_5]^{7-}$ and $[\text{FeO}_6]^{9-}$ units, in the novel iron-based compound: BaYFeO_4 , *Inorg. Chem.* **52**, 2671 (2013).
- [12] C. M. Thompson, J. E. Greedan, V. O. Garlea, R. Flacau, M. Tan, P. H. T. Nguyen, F. Wrobel, and S. Derakhshan, Partial spin ordering and complex magnetic structure in BaYFeO_4 : A neutron diffraction and high temperature susceptibility study, *Inorg. Chem.* **53**, 1122 (2014).
- [13] J. Z. Cong, S. P. Shen, Y. S. Chai, L. Q. Yan, D. S. Shang, S. G. Wang, and Y. Sun, Spin-driven multiferroics in BaYFeO_4 , *J. Appl. Phys.* **117**, 174102 (2015).
- [14] S. Ghara and A. Sundaresan, Coexistence of long-range cycloidal order and spin cluster glass state in the multiferroic BaYFeO_4 , *J. Phys. Condens. Matter* **30**, 245802 (2018).
- [15] I. S. Glazkova, A. A. Belik, A. V. Sobolev, M. N. Smirnova, N. S. Ovanesyan, and I. A. Presniakov, Modulated magnetic structures in BaRFeO_4 ($R = \text{Y}$ and Dy): Magnetic and ^{57}Fe Mössbauer investigations, *J. Phys. Chem. C* **124**, 13374 (2020).
- [16] D. P. Kozlenko, N. T. Dang, R. P. Madhogaria, L. T. P. Thao, S. E. Kichanov, N. Tran, D. T. Khan, N. Truong-Tho, T. L. Phan, B. W. Lee *et al.*, Competing magnetic states in multiferroic BaYFeO_4 : A high magnetic field study, *Phys. Rev. Mater.* **5**, 044407 (2021).
- [17] A. Dönni, V. Y. Pomjakushin, K. Yamaura, and A. A. Belik, Cycloidal spiral magnetic structures in the spin-chain compounds BaRFeO_4 ($R = \text{Yb}$ and Tm): Ordered Yb versus partly ordered Tm, *Phys. Rev. B* **107**, 134412 (2023).
- [18] P. Fischer, G. Frey, M. Koch, M. Könnicke, V. Pomjakushin, J. Schefer, R. Thut, N. Schlumpf, R. Bürge, U. Greuter *et al.*, High-resolution powder diffractometer HRPT for thermal neutrons at SINQ, *Phys. B: Condens. Matter* **276–278**, 146 (2000).
- [19] B. T. M. Willis, Absorption coefficients for neutrons, in *International Tables for Crystallography*, edited by E. Prince (International Union of Crystallography, Chester, 2006), Vol. C, Chap. 4.4, Sect. 4.4.6, p. 461.
- [20] J. Rodriguez-Carvajal, Recent advances in magnetic structure determination by neutron powder diffraction, *Physica B* **192**, 55 (1993).
- [21] L. W. Finger, D. E. Cox, and A. P. Jephcoat, A correction for powder diffraction peak asymmetry due to axial divergence, *J. Appl. Cryst.* **27**, 892 (1994).
- [22] B. J. Campbell, H. T. Stokes, D. E. Tanner, and D. M. Hatch, ISODISPLACE: A web-based tool for exploring structural distortions, *J. Appl. Crystallogr.* **39**, 607 (2006); Information on the program ISODISTORT is described in the following <https://stokes.byu.edu/iso/isodistort.php>.
- [23] K. Momma and F. Izumi, VESTA 3 for three-dimensional visualization of crystal, volumetric and morphology data, *J. Appl. Cryst.* **44**, 1272 (2011).
- [24] See Supplemental Material at <http://link.aps.org/supplemental/10.1103/PhysRevB.109.064403> for figures of the magnetic susceptibility and neutron diffraction data of BaErFeO_4 .
- [25] V. Y. Pomjakushin, M. Kenzelmann, A. Dönni, A. B. Harris, T. Nakajima, S. Mitsuda, M. Tachibana, L. Keller, J. Mesot, H. Kitazawa *et al.*, Evidence for large electric polarization from collinear magnetism in TmMnO_3 , *New J. Phys.* **11**, 043019 (2009).
- [26] A. W. Hewatt, Design for a conventional high-resolution neutron powder diffractometer, *Nucl. Instrum. Methods* **127**, 361 (1975).
- [27] V. Yu. Pomjakushin, D. V. Sheptyakov, K. Conder, E. V. Pomjakushina, and A. M. Balagurov, Effect of oxygen isotope substitution and crystal microstructure on magnetic ordering and phase separation in $(\text{La}_{1-y}\text{Pr}_y)_{0.7}\text{Ca}_{0.3}\text{MnO}_3$, *Phys. Rev. B* **75**, 054410 (2007).